

# An open source, wireless capable miniature microscope system

William A Liberti III<sup>1,2</sup>, L Nathan Perkins<sup>1,2</sup>, Daniel P Leman<sup>1</sup>  
and Timothy J Gardner<sup>1,2,3</sup>

<sup>1</sup> Department of Biology, Boston University, Boston, MA 02215, United States of America

<sup>2</sup> Graduate Program in Neuroscience, Boston University, Boston, MA 02215, United States of America

<sup>3</sup> Department of Biomedical Engineering, Boston University, Boston, MA 02215, United States of America

E-mail: [timothyg@bu.edu](mailto:timothyg@bu.edu)

Received 7 December 2016, revised 8 March 2017

Accepted for publication 21 March 2017


Published 17 May 2017



## Abstract

**Objective.** Fluorescence imaging through head-mounted microscopes in freely behaving animals is becoming a standard method to study neural circuit function. Flexible, open-source designs are needed to spur evolution of the method. **Approach.** We describe a miniature microscope for single-photon fluorescence imaging in freely behaving animals. The device is made from 3D printed parts and off-the-shelf components. These microscopes weigh less than 1.8 g, can be configured to image a variety of fluorophores, and can be used wirelessly or in conjunction with active commutators. Microscope control software, based in Swift for macOS, provides low-latency image processing capabilities for closed-loop, or BMI, experiments. **Main results.** Miniature microscopes were deployed in the songbird premotor region HVC (used as a proper name), in singing zebra finches. Individual neurons yield temporally precise patterns of calcium activity that are consistent over repeated renditions of song. Several cells were tracked over timescales of weeks and months, providing an opportunity to study learning related changes in HVC. **Significance.** 3D printed miniature microscopes, composed completely of consumer grade components, are a cost-effective, modular option for head-mounting imaging. These easily constructed and customizable tools provide access to cell-type specific neural ensembles over timescales of weeks.

Keywords: neurophotonics, optics, freely behaving, calcium imaging, miniature microscope


 Supplementary material for this article is available [online](#)

(Some figures may appear in colour only in the online journal)

## 1. Introduction

Optical recording of neural activity in the brains of behaving animals has become an essential method in systems neuroscience. Through the use of genetically encoded calcium indicators, the principles of learning can be studied in large ensembles of neurons over timescales of weeks and months (Ziv *et al* 2013, Cai *et al* 2016, Liberti *et al* 2016). An

increasingly widespread and powerful method employs miniature head-mounted fluorescence microscopes to record cellular resolution activity in freely moving animals (Ghosh *et al* 2011, Park *et al* 2011, Barbera *et al* 2016). A variety of miniature head-mounted microscopes are available commercially, and the technique has been adopted by many labs (Betley *et al* 2015, Rubin *et al* 2015), but these off-the-shelf devices currently lack a number of desirable features such as easy modification, wireless interfacing, color sensors, and flexible real-time analysis software. Some exciting custom built and/or open-source options have emerged (Barbera *et al* 2016, Cai *et al* 2016), but the need remains for simple modular designs

 Original content from this work may be used under the terms of the [Creative Commons Attribution 3.0 licence](#). Any further distribution of this work must maintain attribution to the author(s) and the title of the work, journal citation and DOI.

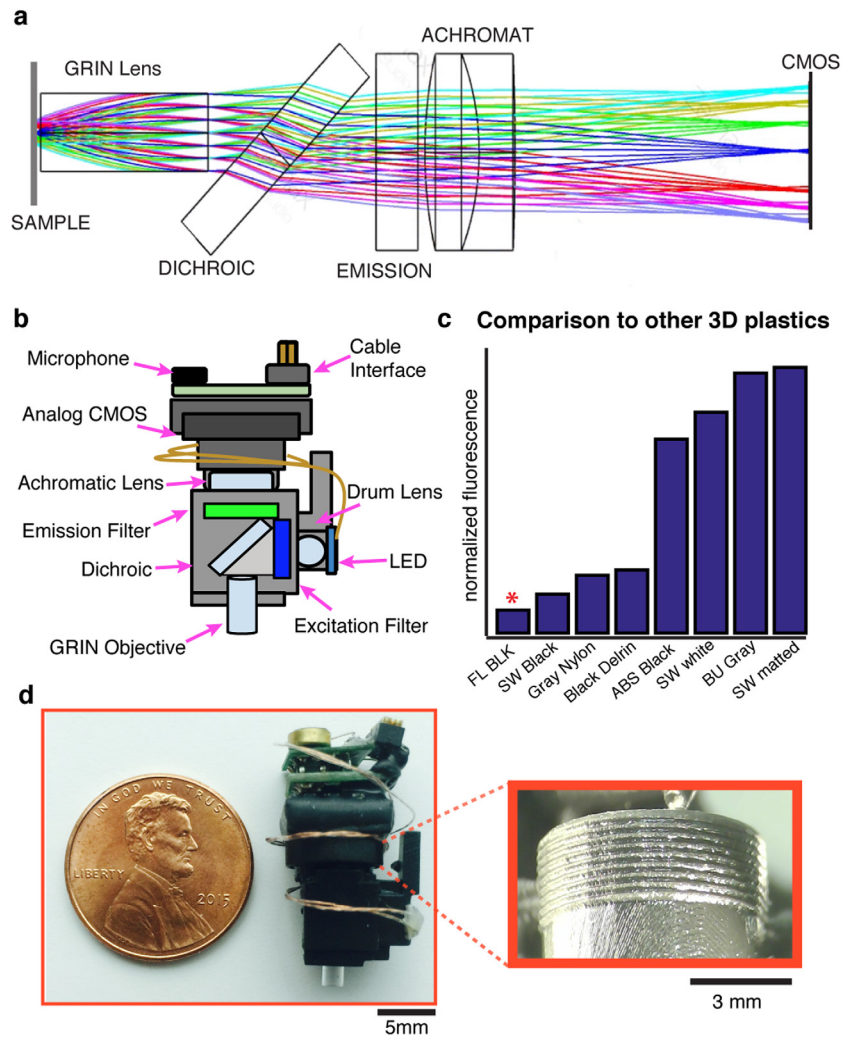


**Figure 1.** A custom 3D printed head-mounted fluorescence microscope. (A) Optical layout of emission pathway for miniature microscope. (B) Microscope schematic. Microscope body is lightweight and robust; CAD design is easily modified. (C) A wide range of 3D printers and plastics were surveyed to maximize resolution and minimize autofluorescence. The red asterisk indicates our final choice of material: Formlab’s Black resin. Autofluorescence of the current design is 1/2 the autofluorescence of black Delrin, one material used for machined microscope designs. (D) Photograph of the microscope produced on a consumer grade 3D printer (Form 2), with inset showing the 3D printed focussing threads with a pitch of 0.34 mm.

that use off the shelf parts and rapid prototyping tools. In our particular application, none of the existing options were sufficiently lightweight for the small animal models employed in our lab. In response, we developed a flexible platform for miniature microscope design and fabrication that could address a variety of experimental needs. New features described in this project include an open-source 3D printed housing for easy experiment-specific reconfiguration, and wireless telemetry. For small animals such as juvenile mice or small songbirds that cannot easily carry the extra weight of the wireless transmitter and battery, we also describe a torque-sensing motorized commutator based on 3D printed parts and low cost hardware. A wired configuration connected through the commutator enables an ultralight configuration for recording (Fee and Leonardo 2001).

In addition to the microscope, this project describes open-source control software capable of low-latency image processing and feedback for closed-loop experiments. Such experiments can trigger stimulation or other feedback in

response to either patterns of recorded neural activity or external analog inputs. As a proof of concept, we demonstrate this capability by performing a closed-loop experiment in which auditory feedback is triggered with precise latency on particular syllables of a zebra finch’s song.

We intend for this project to act synergistically with other emerging open-source neurophotonic efforts (e.g., miniscope.org), to bring these new tools to larger user base and provide a platform for innovative optical recording techniques across the wider scientific community.

## 2. Methods

### 2.1. General miniature microscope design

The microscope design was partially based on a previously described optical pathway, see figure 1(A) (Ghosh *et al* 2011). These miniature microscopes use a gradient refractive index (GRIN) lens as a high quality, short focal length

objective lens. This design takes advantage of the off-axis focusing properties of these lenses, enabling fine focus adjustments post implant. We performed our original experiments with a green fluorescence indicator (GCaMP6) and chose our standard filters accordingly. A blue LED produces excitation light (470nm peak, LUXEON Rebel), powered by a microcontroller. A drum lens (Edmund Optics, NT45-549) directs the LED emission, which passes through a 4 mm  $\times$  4 mm excitation filter (Chroma, bandpass filter, 480/40nm, 4 mm  $\times$  4 mm  $\times$  1.05 mm), deflects off a dichroic mirror (Chroma, 500 BS, 4 mm  $\times$  4.8 mm) and enters the imaging pathway via the gradient refractive index (GRIN) objective lens (GRINtech, GT-IFRL-200, 0.245 pitch length, 0.45 numerical aperture, or Edmund Optics 1.8mm Dia, 670nm DWL, 0.23 pitch length, VIS Coated, GRIN Lens). Fluorescence from the sample returns through the objective, the dichroic, the emission filter (Chroma, bandpass filter, 535/50nm, 4 mm  $\times$  4 mm  $\times$  1.05 mm) and an achromatic doublet lens (Edmund Optics, NT45-207,  $f=15, 12.5$  or 10 mm) that focuses the image onto the CMOS. This sensor is described in greater detail below. The frame rate of the camera is 30 Hz, and the field of view, when using a 15 mm achromat, is approximately 800  $\mu\text{m}$   $\times$  600  $\mu\text{m}$ .

The microscope housing is provided in the common STL format. Various 3D printing resins were screened for their light blocking capacity, minimum print resolution, and auto-fluorescence in response to imaging wavelengths. We surveyed ten 3D printer and plastic combinations to find a low cost, high quality print option. We chose to build our microscope using a commercially available, consumer grade desktop 3D printer (Formlabs Form 2, resin type FGPBLK01 and FGPBLK02). The material has half the autofluorescence as Delrin in the green emission channel (480 nm excitation, 510 nm emission). Other materials surveyed include black acrylic-like resin (Shapeways), opaque acrylic-like resin (Shapeways), Black Delrin (DuPont), Black Nylon (Shapeways), ABS-black (Realize inc), ABS-P430 Ivory (UPrint) and VeroBlack Matte (Objet) (figure 1(C)). With the Form 2 printer, parts can be printed with extremely small feature size (25  $\mu\text{m}$  layers, 140  $\mu\text{m}$  laser spot size), which allows for printing high-resolution threads used to adjust the focal length, as shown in figure 1(D).

## 2.2. Software design

Custom image acquisition software running on the macOS operating system leverages native AVFoundation frameworks to communicate with a USB frame grabber and capture a synchronized audio-video stream (figure 2). Video and audio are written to disk in MPEG-4 container files with video encoded at full resolution using either H.264 or lossless MJPEG Open DML codecs and audio is encoded using the AAC codec with a 48 kHz sampling rate. Data on the regions of interest, fluorescence and triggered feedback are simultaneously written to a table (CSV) that includes corresponding frame numbers. In addition, the software communicates with a microcontroller (Arduino 2560 Mega) via a USB-to-serial connection. The microcontroller board allows the software to control LED brightness, as well as interface with other analog and digital signals.

## 2.3. Near-real-time software details

The software is able to perform near real-time analysis on both the video stream as well as two independent analog channels. Sampled at 48 kHz, these can be used for analog inputs such as audio, TTL pulses, electrophysiology or data about behavioral context. These channels are used for low-latency data collection and triggering, with precise video alignment. For our songbird experiments, one of these channels is used for audio recording and song detection. For example we activate the microscope's LED only during singing, restricting photobleaching and streamlining data collection. For this functionality, the audio stream is processed through a short-time Fourier transform to identify spectral content consistent with singing.

Either the analog input or the video stream can be the substrate for near-real time computational analysis. This allows feedback to be selectively triggered during activity of interest on the video or analog channels. In the case of video analysis, the uncompressed video stream is processed to extract fluorescence information for predefined regions of interest. Figure 2 shows an example of how the software can be used with a predefined triggering rule that applies feedback contingent on fluorescence signals measured in specific ROIs. In this paradigm, the camera can be used as a brain machine interface (BMI) in which songbirds control sounds directly through the measured calcium signals in the brain (Clancy *et al* 2014). Other applications of the software could include closed-loop stimulation experiments that seek to electrically or optically disrupt patterns of activity in real-time.

Figure 2(C) depicts time between LED onset and feedback in our software testbed. The average time to trigger a feedback stimulus is 23.9 ms  $\pm$  7.9 ms (95% confidence interval), including frame exposure, digitization, transmission, data acquisition and software processing. This latency reflects the intrinsic limitations of the 30 FPS (33 ms) frame rate as well as time spent capturing and decoding video, and communicating an output TTL with the Arduino controller through the serial port. Data acquisition, region of interest processing, and feedback triggering all occur within an average of 1.7 ms after frame capture (95% confidence: <11 ms). This variability stems primarily from video encoding and storage, where the codec and write buffering necessitate increased processing time for a subset of frames. An additional source of variability in processing time, which has a smaller impact and is shown in figure 2(D), relates to the number and complexity of the defined regions of interest. As the number and size of the regions of interest increases, the processing time increases. In tests involving ten cell-sized regions of interest, the average processing time was 0.17 ms with a range of 0.11 ms–0.22 ms (95% confidence interval).

## 2.4. Auditory feedback

To test the acquisition pipeline for triggering on behavior, we used the integrated microphone on the head mounted microscopes to detect specific syllables of a bird's song and deliver white noise auditory feedback at specific delays after the syllable was produced. White noise bursts are a common aversive

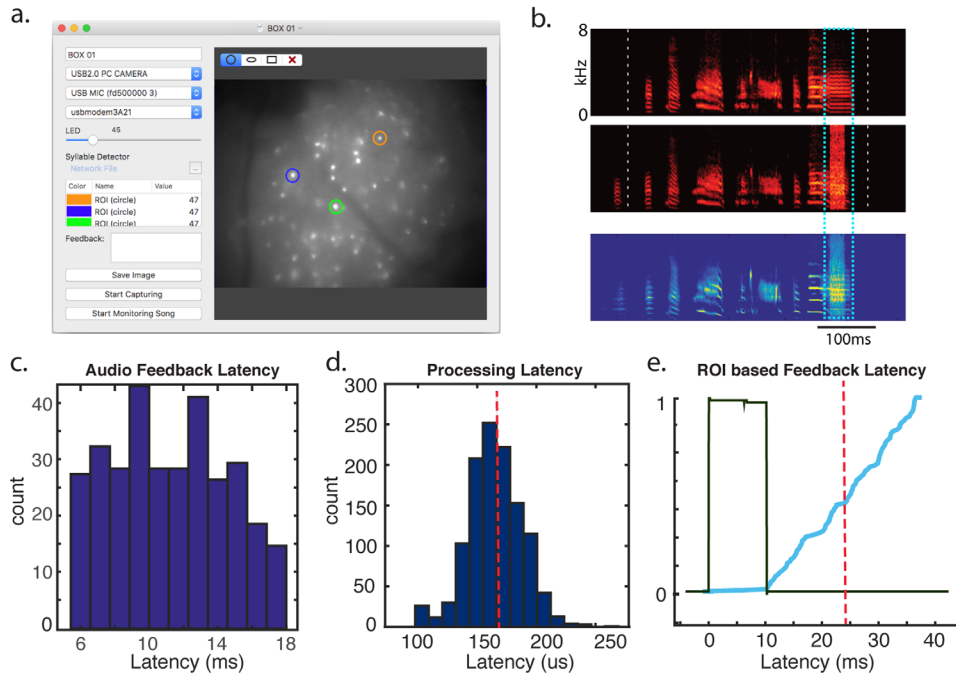


**Figure 2.** Performance of closed loop feedback based on near real-time audio or image processing using custom software and GUI. (A) Image of user interface of acquisition software written in Swift for macOS. The software allows for low-latency ROI tracking and microscope control. It also interfaces with a microcontroller with 54 digital I/O pins, 16 8 bit analog inputs and an ADC with two tightly synchronized 16 bit 48 kHz analog inputs (typically for audio). (B) Example of feedback contingent on features of the audio input: white noise is triggered at a specific syllable of song. White dotted lines mark a single motif of song, blue indicates the target syllable. *Top*: a ‘catch’ trial, where no feedback was delivered. *Middle*: a ‘hit’ trial, where a 50 ms white noise pulse was delivered. *Bottom*: spectral density image of all song aligned trials (including hit and catch trials), demonstrating the reliability of the white noise pulse. (C) Latency of auditory-based feedback, from singing of a specific syllable to TTL pulse from detector, was  $12 \text{ ms} \pm 6 \text{ ms}$ . (D) Of the total latency, image processing to extract fluorescence from ten cell-sized regions of interest contributes an average of only 0.17 ms; much of the ROI feedback latency is a reflection of the frame rate and acquisition time. (E) Example of feedback contingent on ROI tracking. Black: voltage driving an LED light flash that is recorded in the field of the CMOS; blue: the cumulative probability density function (CDF) of a brief TTL pulse triggered by the software in response to the LED flash processed through the entire acquisition system. Event detection was based on ROI analysis on a Mac Mini computer. Latency of the full loop from camera to Arduino based TTL output is approximately  $23.9 \text{ ms} \pm 7.9 \text{ ms}$  (95% confidence interval), with the jitter comparable to the frame rate of the camera. In this test, the LED was not synchronized to the onset of the frame, as would be the case for spontaneous video recording of neural activity. This represents the experimentally relevant performance of the system, intrinsically limited by the 33 ms frame rate of the camera.

stimulus for differential reinforcement in songbirds because it obscures normal feedback that the bird experiences (Tumer and Brainard 2007, Andalman and Fee 2009). Custom Swift software was used for online detection of target syllables. White noise bursts were delivered at precise times relative to the target syllable during the bird’s vocalization. The duration of white noise bursts was long enough to overlap with the remainder of the targeted syllable (50 ms). This feedback was delivered with minimal trial to trial jitter, on the order of  $12 \text{ ms} \pm 6 \text{ ms}$  latency from the target syllable, using a neural-network-based syllable detector (Pearre *et al* 2016).

## 2.5. CMOS sensor and wireless transmitter

The choice of CMOS imaging sensor is flexible. Benchtop systems and existing commercial solutions have employed a high definition (HD) resolution sensor with on-board digitization in the microscope. However, due to out-of plane fluorescence, the resolution of single photon imaging *in vivo* is typically much lower than the Nyquist sampling of a HD CMOS. At HD resolution, spatially oversampled images can result in a

cumbersomely large file size that hinders data processing on conventional lab computers—as a result, it is common for processing pipelines to start with spatial downsampling. Given the limited value in HD resolution for our application, we chose to start with a lower resolution sensor having only  $640 \times 480$  pixels, a design choice that provided other benefits. Specifically, this lower resolution frame can be transmitted through a variety of low-cost, compact wireless transmitters, as shown in figure 3. The NTSC video protocol we use here is a mature technology incorporated into many low cost devices such as wireless spy cameras or miniature cameras for remote control airplanes. The same format also allows for analog transmission via flexible tethers for use in small songbirds or juvenile mice. The system can be appropriately employed *in vivo* as demonstrated by minimal degradation over timescales used in realistic experiments (see figures 3(D) and (E)) and by normal behavior of animals wearing the microscope (supplemental video 5 ([stacks.iop.org/JNE/14/045001/mmedia](http://stacks.iop.org/JNE/14/045001/mmedia))). However, the greatest utility will be in animals where a wired option is not possible or feasible, such as in behaving bats or crows, or where a data cable might restrict normal behavior.



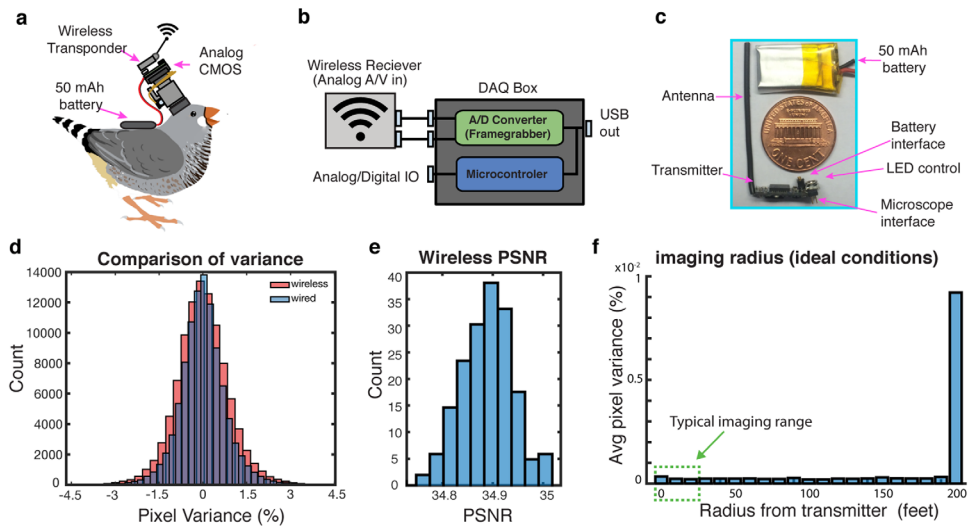


**Figure 3.** Wireless microscope acquisition system and performance. Signals from the camera can be relayed with an off-the-shelf wireless transmitter. (A) Diagram of the system, mounted on a songbird. The microscope LED, CMOS and transmitter together draw approximately 100 mA, at the typical input voltage of 3.5 V and the typical *in vivo* imaging LED brightness. (B) The wireless acquisition system uses a wireless receiver, frame-grabber and digitizer to acquire synchronized video and two channels of 48 kHz audio. (C) Image of wireless transmitter and 50 mAh battery. (D) Comparison of pixel noise in the wired and wireless conditions (see methods 2.8.3). (E) Histogram of per-frame PSNR values of the wireless condition, as compared to the wired condition (at 3 m). (F) Variance of the mean pixel value, over 100 continuously recorded frames (per distance). High variance indicates signal degradation due to transmission loss or interference. Over distances relevant for typical neuroscience applications in an indoor laboratory setting, these transmitters are subject to minimal signal degradation.

The camera circuit employed for the microscopes in this study is an off-the-shelf integrated color CMOS camera system (3rd eye electronics, MC900). It uses a 1/3" color CMOS (OV7960 TSV). Each on-chip pixel is 6  $\mu\text{m}$ , and the signal to noise ratio (SNR) for the camera is 52 dB, with a sensitivity of 0.008 Lux. The camera circuit is also available with an integrated microphone (MC900A). The circuit draws less than 70 mA with an operating voltage of 3.3–5 V. A total of five wires run from the microscope—one wire each for camera power, ground, audio, NTSC analog video, and LED power. These wires run through a custom flex-PCB interconnect (Rigiflex) up to a custom-built active commutator (described in greater detail below). The NTSC video signal and analog audio are digitized through a USB frame-grabber. The integrated video frame-grabber and analog-to-digital converter (AV2USB\_V1.4, or DM420) converts two channels of 48 kHz analog data (in the case of songbirds, used for audio) and a synchronized NTSC video stream for reading by the host computer. While the color NTSC cameras provide wireless and color imaging, it potentially results in lower SNR in the GFP band. This may not be ideal for some applications—fortunately, the CMOS is easily changed for users that do not require color or wireless recording.

Off-the-shelf wireless transmitters are available for the NTSC format audio/video, and weigh less than 0.6 g (e.g. BOSCAM TX24019, or many others) figure 3(C). These transmitters perform reliably over distances of 5 m or more, a measure confirmed in figure 3(E). The small scale and relatively low power requirements of the transmitter make them an attractive modification for untethered recording in freely moving animals. In our tests, we powered the device with a lightweight, consumer grade lithium polymer (LiPo)

battery. The choice of battery depends on weight constraints of the animal species: we have tested small, 1 g 50 mAh batteries for functional use up to 30 min, and 3 g 105 mAh batteries for up to an hour, at average imaging LED intensities. The microscope weighs 1.8 g and the 50 mAh battery and transmitter adds an additional  $\sim 2$  g. This combination was burdensome for most zebra finches, although they are able to carry the complete system (see supplemental video 5). The wireless system is ideal for larger animals, such as bats, rats or crows, that can carry the additional weight. We have also had success in using this system in mice (unpublished observations).

## 2.6. Commutator design

To image in songbirds, which were unable to carry the extra weight of the battery and wireless transmitter, we developed a torque-sensing 3D printed commutator (figure 4(A)), as well as lightweight, ( $\sim 0.1$  g) low-noise, flexible PCB cables. The commutator was inspired by previous designs (Fee and Leonardo 2001). These commutators allowed for 24/7 longitudinal recording without frequent handling of the animals. The ability to record longitudinally from animals may prove useful in larger animals as well, as it avoids the complexity of battery management and charging.

The active commutator consists of a gear assembly (ABS-P430 Ivory, UPrint), along with seven electronic components that can be purchased for a total cost of under \$100. These additional components include a servo and a resistor, a slip ring commutator, a disk magnet and a hall sensor (figure 4(C)). The mechanical designs, editable

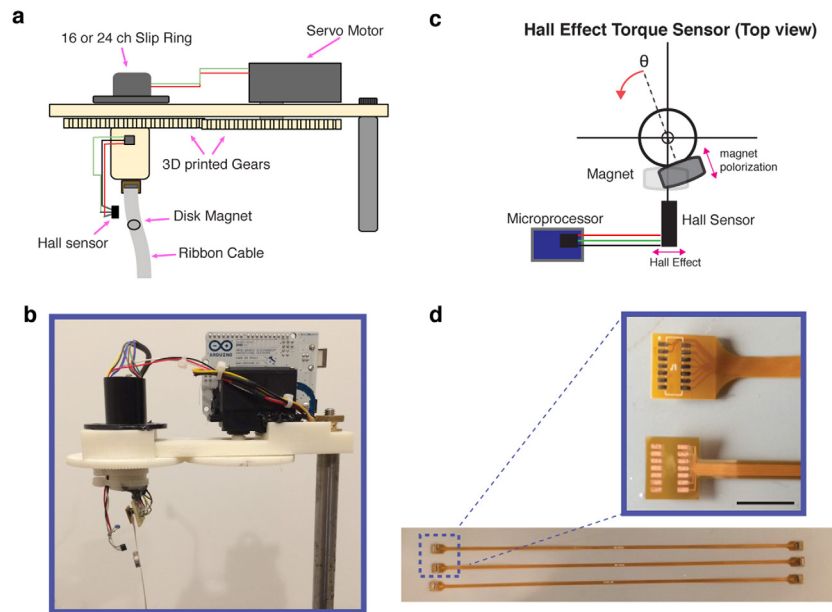


**Figure 4.** 3D printed active commutator system for chronic neural recording in small animals. (A) Schematic of the 3D printed commutator. (B) An image of an assembled commutator. (C) These devices use the deflection of the magnetic field of a disk magnet located on a flex PCB cable to detect torque via a hall sensor. A feedback circuit mediated by a microcontroller corrects the deflection by rotating a slip ring via a servo-driven gearbox with a 1:1 ratio. (D) Example of two different flex cables designs with 7–9 conductors, weighing under 0.25 g. The additional wires are present for electrical/optical stimulation or other head-mounted accessories. Scale bar indicates 9 mm.

stereolithography designs, and software to operate the commutator is included in the supplement.

## 2.7. Surgical procedure

To label neurons in the song-related premotor nucleus HVC with a calcium indicator, birds received three 250 nl injections of lentivirus packaged with either GCaMP6s or GCaMP6f under a Rous sarcoma virus (RSV) promoter. Virus is prepared as described previously (Liberti *et al* 2016), and constructs are available in Addgene ([www.addgene.org/Darrell\\_Kotton/](http://www.addgene.org/Darrell_Kotton/)). To guide the injection of virus, the boundaries of HVC were determined by fluorescence targeting of a DiI retrograde tracer injected into the downstream song motor nucleus Area X.

## 2.8. Data analysis

**2.8.1. Song alignments.** For all neural recording modalities, trials were aligned to song using previously described methods (Poole *et al* 2012), using the Euclidean distance in spectral features between the data and a template song in a sliding window. Local minima in the Euclidean distance were considered candidate hits, which were then plotted in 2 dimensions for the user to perform a cluster cut. No time warping was applied to any data (Glaze and Troyer 2006).

**2.8.2. Calcium imaging ROI analysis.** Calcium imaging data was analyzed as described previously (Markowitz *et al* 2015). In brief, raw imaging data was motion corrected using a previously published algorithm (Guizar-Sicairos *et al* 2008). Then, regions of interest (ROIs) were manually selected, and for

each frame, pixels intensities were averaged for all pixels in the region. ROI traces were converted to  $\Delta F/F_0$  by estimating  $F_0$  as the 12th percentile in an 800 ms sliding window.

**2.8.3. Wireless imaging quality quantification.** Wireless imaging data quality was assessed by splitting the analog NTSC video signal into two paths: one to a wired frame-grabber, and the other through a wireless transmitter and receiver, to a second frame-grabber. This allows for explicit evaluation of the image quality for the same video stream, enabling frame-by-frame comparison of the wireless and wired conditions. The differences between frames encompasses both signal degradation due to wireless encoding, and noise introduced due to interference from other devices, giving a practical measurement of signal degradation. These experiments were performed in realistic lab conditions with a clear path from transmitter to receiver, but no additional steps were taken to mitigate potential sources of noise.

## 3. Results

### 3.1. Optical recording of neurons expressing genetically encoded calcium indicators

To provide information about excitatory cells, we used our miniature microscopes to perform optical imaging of neurons expressing genetically encoded calcium indicators (figure 5) (Markowitz *et al* 2015, Liberti *et al* 2016). Electrophysiology methods are typically unable to track individual neurons over long time periods. Excitatory projection cells in this region are extremely difficult to continuously record for timescales longer than a single day, perhaps due to limitations of recording from

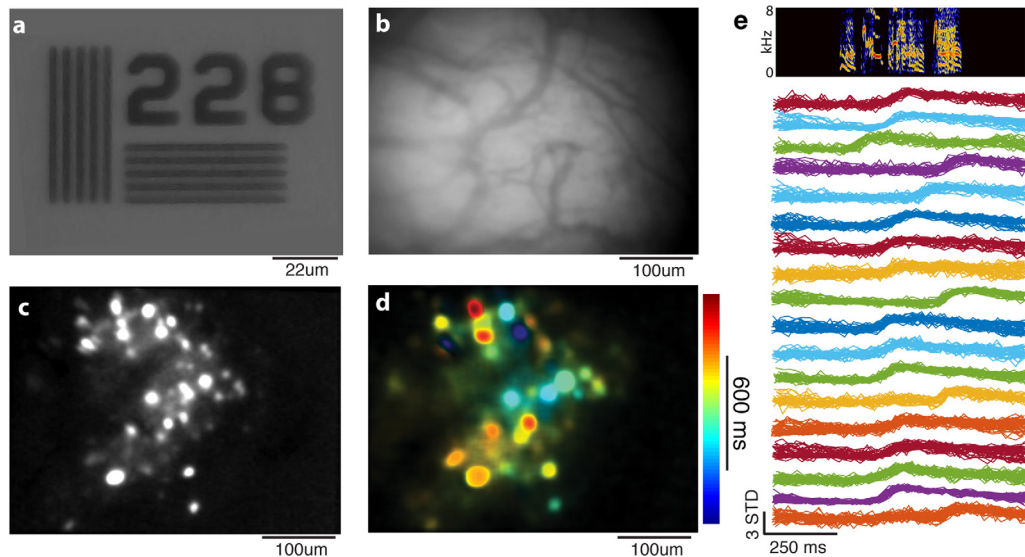


**Figure 5.** Images and *in vivo* video collected from the microscope. (A) Image taken by microscope of a High-Frequency NBS 1963A Resolution Test Target, showing 228 lines per mm. (B) *In vivo* widefield image of blood vessels over premotor area HVC in a zebra finch. (C) Maximum intensity projection of  $\Delta F/F_0$  video from a bout of singing. Imaging depth is 150–200  $\mu\text{m}$  below the surface of intact dura. (D) Time-intensity plot, where each pixel is colored by its center of mass in time. (E) Stereotyped single neuron calcium traces recorded in singing birds using GCaMP6, aligned to song. *Top*: spectrogram of a single song rendition; *bottom*: calcium traces from 18 ROIs over 50 song-aligned trials from a single bird. Vertical scale bar indicates standard deviation.

smaller cells (Guitchounts *et al* 2013). As a proof of concept, we optically recorded the fluorescence transients from neurons expressing the calcium indicator GCaMP6 in the songbird premotor cortex HVC. Consistent with previous extracellular recordings and calcium imaging studies in HVC, projection neuron calcium activity patterns were highly stereotyped and stable across song trials within a day of singing, as shown in figure 5(A). Microvasculature can be clearly seen in figure 5(B) above HVC on the surface. Cells were identified that produced stereotyped calcium transients at all time-points within song, and displayed characteristic spatiotemporal organization (Markowitz *et al* 2015). Within a song rendition, dozens of cells can be recorded simultaneously. Because these microscopes are lightweight and inexpensive, they can be chronically implanted and left in place for weeks at a time. This provides a paradigm for stable longitudinal recordings.

#### 4. Discussion

Cellular resolution optical imaging in behaving animals is a foundational method in modern neuroscience—allowing researchers to longitudinally track cells in sparsely active networks like the songbird premotor region HVC and the rodent hippocampus with high spatial resolution. Through the use of genetically encoded calcium indicators (Chen *et al* 2013, Dana *et al* 2016), the principles of learning, information encoding, etc, can be studied in large ensembles of neurons at cellular resolution, over periods of weeks and months. Typically, optical experiments utilize either benchtop two-photon imaging systems in head-restrained animals (Dombeck 2010, Rickgauer *et al* 2014, Minderer *et al* 2016), or single photon imaging in freely moving animals through the use of a head-mounted miniature fluorescence (single photon) microscope

(Ghosh *et al* 2011, Park *et al* 2011, Barbera *et al* 2016, Cai *et al* 2016). While the axial resolution of multiphoton microscopy is vastly superior (Helmchen and Denk 2005), head-mounted microscopes are often the only way to optically observe neural populations during naturalistic behaviors (Resendez *et al* 2016).

The motivation for this project was that existing commercially-available miniature microscopes proved too heavy to consistently evoke undirected song, a learning-intensive motor behavior in zebra finches. With extensive screening and training of birds, it is possible to evoke song in a head-fixed preparation in the presence of a mate (Picardo *et al* 2016), but this approach can be low yield since few birds will sing head-fixed, and the method may preclude the study of the mechanisms of motor maintenance that occur during undirected singing in the absence of a female. More generally, there are many applications in neuroscience where even a wire tether may restrict natural behavior and prevent interrogation of the underlying neural mechanisms (Yartsev and Ulanovsky 2013, Wiltschko *et al* 2015). Songbirds wearing commercially available microscopes rarely sing—possibly due to the microscope weight or bulky cables used to stream data from the CMOS. With the torque sensing commutator and lightweight tether, our present design is sufficiently unobtrusive for zebra finches; we routinely gather 400–1000 song motifs per day. This microscope system, in conjunction with behaviorally triggered acquisition has allowed us to perform around-the-clock studies of brain activity in a substantial number of animals without constant human supervision, enabling us to gather densely sampled longitudinal recordings. The tool will enable further studies of learning at cellular resolution in zebra finches (figure 5). This development history and outcome underscores a limitation of commercial solutions: while off-the-shelf versions may provide adequate



functionality for some species or experimental paradigms, many experiments require user-defined customization. It is likely that modifications described here, such as wireless interfacing, custom filter sets, and color sensors, as well as the modular design of this miniature microscope will inspire innovation and enable data collection in new experimental models or species.

#### 4.1. Advantage of 3D printed housing for rapid microscope assembly and prototyping

Existing miniature microscope designs require assembly of carefully machined parts, typically milled from Peek or Delrin plastic (Ghosh *et al* 2011, Cai *et al* 2016). These machined parts have the advantage of precise tolerances, but also have the disadvantage of higher cost and longer design timescales relative to 3D printed materials. 3D printed microscopes can be produced at low cost with geometries that are not possible with CNC milling—we take advantage of a single-piece design that reduces weight by eliminating metal bolts and allowing thin walls. Because 3D printed parts avoid the constraints of machined parts, these microscopes can be lighter, more easily constructed, and readily reconfigurable to accommodate design variations.

#### 4.2. All optical physiology with multi-channel light delivery and recording

While we ran initial tests with filters optimized for imaging GCaMP6, different filter sets can be used to accommodate newer, red-shifted indicators. With some modifications, these cameras can be adapted to incorporate two independent color channels at the expense of SNR within each channel. Optimization of filter sets and incorporating multi-wavelength spectral peak LEDs can provide additional information about cells in the imaging plane, using fluorescent proteins or tracers with well-isolated spectral profiles to differentially label subpopulations of cells. Examples include GCaMP6 combined with infrared Alexa dyes for retrograde labelling. This additional channel can allow disambiguation of specific neuron types within an imaging field. Alternatively, adding a second pass to the dichroic and excitation filter can allow full field optical stimulation outside of the imaging bands.

#### 4.3. Low latency, open source acquisition software

In our tests, the latency of triggering off fluorescence activity was limited by the framerate of the microscope, about  $23.9\text{ms} \pm 7.9\text{ms}$  (figure 2(C)). For many experiments, this response latency is acceptable. In the songbird, for example, the sensory-motor latency from pre-motor neuron activity in HVC to auditory sensory consequences processed in the basal ganglia is a minimum of 32–50 ms (Andalman and Fee 2009). Based on these estimates and published accounts of conditional feedback experiments in songbirds, the time-delay should provide a learnable brain machine interface (Oliveczky *et al* 2005, Tumer and Brainard 2007, Sakata and Brainard 2008, Sober and Brainard 2009). However it remains to be

seen whether the timing jitter in the current system is acceptable for brain machine interface experiments in a system as precise as the songbird. For the zebra finch, relative jitter between premotor commands and auditory feedback is just a few milliseconds. For some experiments, lower latency and lower variability may be desirable, and with the introduction of faster frame rate cameras and deterministic real-time operating systems, this latency and latency variability will decrease.

#### 4.4. CMOS trade-offs and deficits

In our tests, we use an off-the-shelf CMOS that outputs analog video. In terms of resolution, shot noise and frame rate, the NTSC analog camera is less versatile than many new digital sensors. These analog protocols do have the advantage of being easily broadcast wirelessly with high signal fidelity and low power consumption, which allows real-time data streaming for wireless BMI experiments, and also allows adjustment of imaging parameters on-the-fly. These sensors have been adequate for calcium imaging experiments—although other experiments may benefit from higher resolution digital sensors (Deisseroth and Schnitzer 2013, Cai *et al* 2016).

#### 4.5. Use of off-the-shelf components for ease of construction

Designing and constructing optical equipment poses engineering challenges—many researchers and educators, especially in resource-limited circumstances, may be intimidated by constructing their own systems. This can especially be the case with custom ASIC or chip design which requires considerable technical skill. With this in mind, we have aimed to present a design that is built from low cost, off-the-shelf components. The design requires minimal maintenance, enabling longitudinal use. This microscope design will allow labs with little electronics experience to enter the field of awake behaving imaging and to build their own microscopes, while providing room for electronics savvy experimentalists to iterate and develop novel imaging and acquisition back ends.

The future development of these devices relies greatly on a combined multidisciplinary effort, involving biological, chemical, mechanical, and material engineering, among others. In particular, neuroscience stands to benefit from advances in consumer grade electronics. The cost, availability, size and quality of electronics used in this project is the result of innovations from the cellular and telecommunications industries (Deisseroth and Schnitzer 2013). This sector will likely continue to drive rapid innovation in miniaturization of electronics, nanoscale 3D printed components (Sun and Kawata 2004) and optics (Gissibl *et al* 2016), and high-fidelity wireless technology—all of which stand to increase the quality and decrease the cost of neuroscience instrumentation. We hope that the microscope presented here will be further enhanced by these efforts and allow maximum integration with other emerging open-source neurophotonics projects.



## Acknowledgments

This effort would not have been possible without the critical advice and support at the outset of the project by Daniel Aharoni and Peyman Golshani. The authors would like to thank the Gardner lab, especially Alejandro Eguren, Carlos Gomez and Ali Mohammed for their help with microscope assembly, as well as Ben Pearre for developing and providing the neural network based syllable detector and Dawit Semu for providing excellent animal husbandry. We would also like to thank Aurelien Begue and Bernardo Sabatini for assistance with ZEMAX modeling and useful discussions. We also would like to thank Derek Liberti and Darrell Kotton for constructing and designing the RSV-GCaMP lentiviral construct. Special thanks to D S Kim and L Looger for providing the GCaMP6 DNA and to the GENIE project at Janelia Farm Research Campus, Howard Hughes Medical Institute. This work was supported by a grant from CELEST, an NSF Science of Learning Center (SBE-0354378) and by grants from NINDS R24NS098536 and R01NS089679.

## References

- Andalman A S and Fee M S 2009 A basal ganglia-forebrain circuit in the songbird biases motor output to avoid vocal errors *Proc. Natl Acad. Sci. USA* **106** 12518–23
- Barbera G et al 2016 Spatially compact neural clusters in the dorsal striatum encode locomotion relevant information *Neuron* **92** 202–13
- Betley J N et al 2015 Neurons for hunger and thirst transmit a negative-valence teaching signal *Nature* **521** 180–5
- Cai D J et al 2016 A shared neural ensemble links distinct contextual memories encoded close in time *Nature* **534** 115–8
- Chen T-W et al 2013 Ultrasensitive fluorescent proteins for imaging neuronal activity *Nature* **499** 295–300
- Clancy K B et al 2014 Volitional modulation of optically recorded calcium signals during neuroprosthetic learning *Nat. Neurosci.* **17** 807–9
- Dana H et al 2016 Sensitive red protein calcium indicators for imaging neural activity *eLife* **5** e12727
- Deisseroth K and Schnitzer M J 2013 Engineering approaches to illuminating brain structure and dynamics *Neuron* **80** 568–77
- Dombeck D A et al 2010 Functional imaging of hippocampal place cells at cellular resolution during virtual navigation *Nature Neurosci.* **13** 1433–40
- Fee M S and Leonardo A 2001 Miniature motorized microdrive and commutator system for chronic neural recording in small animals *J. Neurosci. Methods* **112** 83–94
- Ghosh K K et al 2011 Miniaturized integration of a fluorescence microscope *Nat. Methods* **8** 871–8
- Gissibl T et al 2016 Two-photon direct laser writing of ultracompact multi-lens objectives *Nat. Photon.* **10** 554–60
- Glaze C M and Troyer T W 2006 Temporal structure in zebra finch song: implications for motor coding *J. Neurosci.* **26** 991–1005
- Guitchounts G et al 2013 A carbon-fiber electrode array for long-term neural recording *J. Neural Eng.* **10** 046016
- Guizar-Sicairos M, Thurman S T and Fienup J R 2008 Efficient subpixel image registration algorithms *Opt. Lett.* **33** 156
- Helmchen F and Denk W 2005 Deep tissue two-photon microscopy *Nat. Methods* **2** 932–40
- Liberti W A III et al 2016 Unstable neurons underlie a stable learned behavior *Nat. Neurosci.* **19** 1665–71
- Markowitz J E et al 2015 Mesoscopic patterns of neural activity support songbird cortical sequences *PLoS Biol.* **13** e1002158
- Minderer M et al 2016 Neuroscience: virtual reality explored *Nature* **533** 324–5
- Olveczky B P, Andalman A S and Fee M S 2005 Vocal experimentation in the juvenile songbird requires a basal ganglia circuit *PLoS Biol.* **3** e153
- Park J H et al 2011 Head-mountable high speed camera for optical neural recording *J. Neurosci. Methods* **201** 290–5
- Pearre B, Perkins N, Markowitz J and Gardner T 2016 A fast and accurate zebra finch syllable detector *PLoS One* (accepted)
- Picardo M A et al 2016 Population-level representation of a temporal sequence underlying song production in the zebra finch *Neuron* **90** 866–76
- Poole B, Markowitz J E and Gardner T J 2012 The song must go on: resilience of the songbird vocal motor pathway *PLoS One* **7** e38173
- Resendez S L et al 2016 Visualization of cortical, subcortical and deep brain neural circuit dynamics during naturalistic mammalian behavior with head-mounted microscopes and chronically implanted lenses *Nat. Protocols* **11** 566–97
- Rickgauer J P, Deisseroth K and Tank D W 2014 Simultaneous cellular-resolution optical perturbation and imaging of place cell firing fields *Nat. Neurosci.* **17** 1816–24
- Rubin A et al 2015 Hippocampal ensemble dynamics timestamp events in long-term memory *eLife* **4** e12247
- Sakata J T and Brainard M S 2008 Online contributions of auditory feedback to neural activity in avian song control circuitry *J. Neurosci.* **28** 11378–90
- Sober S J and Brainard M S 2009 Adult birdsong is actively maintained by error correction *Nat. Neurosci.* **12** 927–31
- Sun H-B and Kawata S 2004 Two-photon photopolymerization and 3D lithographic microfabrication *NMR 3D Analysis Photopolymerization (Advances in Polymer Science)* (Berlin: Springer) pp 169–273
- Tumer E C and Brainard M S 2007 Performance variability enables adaptive plasticity of ‘crystallized’ adult birdsong *Nature* **450** 1240–4
- Wiltschko A B et al 2015 Mapping sub-second structure in mouse behavior *Neuron* **88** 1121–35
- Yartsev M M and Ulanovsky N 2013 Representation of three-dimensional space in the hippocampus of flying bats *Science* **340** 367–72
- Ziv Y et al 2013 Long-term dynamics of CA1 hippocampal place codes *Nat. Neurosci.* **16** 264–6